3. 実験

実験に使用するモデルは実際の CT 像から膵臓，肝臓尾状葉，周囲の血管を抽出し，3D プリンタ (uPrint SE, Stratasys 社)により作成した (Fig. 1). また，大局レジストレーションに用いる基準点をモデルの周囲に，レジストレーション誤差を評価する評価点を血管上に配置した．

実験では，実際の手術時に発生するレジストレーション誤差を模擬するため，大局レジストレーション後にモデルの位置を変化させる．その後局所レジストレーションを行い評価点での誤差の変化を計測する．具体的には以下の a~f の手順で実験を行った．

a. 臓器モデルの基準点 4 点の 3 次元座標を光学式位置センサにより取得．
b. 基準点を用いた CT-センサ座標系の大局レジストレーションを実行．
c. 臓器モデルの移動(頭尾左右のいずれかの方向へ 20mm 移動させ，右方向から頭方向に向かって約 15 度の回転)．これによりレジストレーション誤差を発生させる．
d. CT 像上の膵臓表面及び肝臓尾状葉表面の座標点群を手動で取得．
e. モデルの膵臓表面及び肝臓尾状葉表面を光学マーカが取り付けられた鉗子でなぞり光学式位置センサにより座標点群取得．
f. 手順 d,e で取得した点群の局所レジストレーションを実行．

手順 e,f の処理を頭尾左右方向の各方向で 5 回ずつ，合計 20 回の実験を行い，評価点における CT-センサ座標系の誤差

$$\mathrm{E} = \mathbf{R}^{*}\mathbf{p}_e + \mathbf{T}^{*} - \mathbf{x}_e \qquad (2)$$

を計測した．ここで，$\mathbf{p}_e, \mathbf{x}_e$はそれぞれセンサ座標系及び CT 座標系の評価点の位置を示し，$\mathbf{R}^{*}, \mathbf{T}^{*}$は局所レジストレーションにより得られた回転行列及び平行移動行列を表す．手順 f における局所レジストレーションは，膵臓表面と肝臓尾状葉表面の両方の点群を用いた場合と膵臓表面のみ及び肝臓尾状葉表面のみの点群を用いた場合の 3 種類を行い，評価点における誤差を比較した．

4. 結果および考察

膵臓表面及び肝臓尾状葉表面のみの点群を用いて局所レジストレーションを行った場合と，膵臓と肝臓尾状葉の両方の点群を用いて行った場合の評価点における誤差を Fig. 2 に示す．局所レジストレーション前の評価点における誤差は平均 21.8mm であったが，Fig. 2 より，膵臓表面及び肝臓尾状葉表面の点群のみを用いた場合では，それぞれ平均 8.6mm と 10.9mm，膵臓と肝臓尾状葉の両方の点群を用いた場合では平均 6.6mm となり，多くの場合において 2 つの臓器表面形状を用

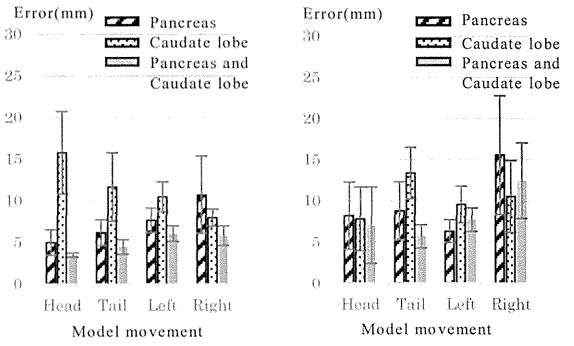

(a) Result on Model 1　　(b) Result on Model 2

Fig. 2 Errors at evaluation points.

いることで誤差が減少した．しかし，モデル 2 においてモデルを左方向へ動かした際には膵臓の点群のみを用いた場合が，右方向へ動かした際には肝臓尾状葉の点群のみを用いた場合が最も誤差が小さくなった．また，モデル 1 とモデル 2 では動かした方向が同じ場合でもその結果は大きく異なった．これは，膵臓や肝臓尾状葉の形状の違い，膵臓と肝臓尾状葉の位置関係，位置センサにより取得した点の分布の違いなど様々な要因が考えられる．今後はさらに多くの症例での実験及び調査の必要があり，また，各臓器の特徴的な形状に重み付けを行うことで，形状の違いがレジストレーション結果に及ぼす影響を少なくすることができると考えられる．

5. むすび

本稿では，複数臓器の表面形状を用いた局所レジストレーション手法を提案した．本手法により，従来手法と比較して誤差を削減することができ，術野におけるレジストレーション精度向上への有効性を確認した．今後の課題として，臓器表面における特徴的な形状部分への重み付けを含むレジストレーション手法の検討があげられる．

謝辞

日頃から熱心に御討論頂く森研究室の諸氏に感謝する．
本研究の一部は，文科省 JSPS 科研費 21103006, 25242047, 26560255, 26108000 ならびに栢森情報科学振興財団研究助成金によった．

文献

1) 森田千尋，林雄一郎，小田昌広，三澤一成，森健策．腹腔鏡下胃切除術の術中ナビゲーションシステムにおける局所レジストレーション手法の開発．第 33 回日本医用画像工学会大会(JAMIT2014)予稿集; PP27.
2) Besl P, Neil D: A method for registration of 3-D shapes. IEEE Transactions on Pattern Analysis and Machine Inteligence 1992;14:239-256.

S05-06　　腹部外科領域における３次元位置センサを用いた術中ナビゲーションシステムの開発と臨床応用

愛知県がんセンター中央病院　消化器外科[1)]，名古屋大学情報科学研究科[2)]，名古屋大学情報連携統括本部[3)]
三澤一成[1)]，伊藤誠二[1)]，伊藤友一[1)]，植村則久[1)]，夏目誠治[1)]，木下敬史[1)]，木村賢哉[1)]，千田嘉毅[1)]，安部哲也[1)]，小森康司[1)]，清水泰博[1)]，木下平[1)]，林雄一郎[2)]，小田昌宏[2)]，森健策[3)]

医用画像処理技術やセンシング技術の進歩は著しく、頭頸部領域や整形外科領域では位置センサなどを用いた手術ナビゲーションシステムが実用化されている。一方、腹部外科手術では対象が変形移動しやすいなどの問題もあり、まったく実用化されていない。我々は2009年より工学系研究者と共同で３次元位置センサを用いた腹腔鏡手術ナビゲーションシステムの開発および臨床応用に取り組んでいる。共同研究者によって開発された画像処理システムにて術前CT画像等から詳細な３次元仮想腹腔内画像（３D-Virtual Laparoscopic Images: ３D-VLI）を作成。さらに光学式位置センサを組み合わせ、腹腔鏡下手術のスコープおよび鉗子に装着した反射球マーカの位置情報を連続的に取得することにより、腹腔鏡術野に応じた３D-VLIの提示や鉗子位置をリアルタイムに表示する術中ナビゲーションを行っている。これまで約40例の腹腔鏡下胃切除術において本システムを使用し手術を行った。手術時間、出血量の減少は認められなかったが、術野に相当する詳細な解剖情報を適宜提示するシステムとして有用であると感じている．術中のシステム操作や、腹壁・臓器が変形移動しやすいことによるレジストレーションおよび表示精度などに課題があり、現在操作インターフェースの開発や、表示精度向上のための研究を継続中である。将来的には腹部外科でも一般臨床応用可能な術中ナビゲーションシステムの開発を目指している。

Investigation of Optimal Feature Value Set in False Positive Reduction Process for Automated Abdominal Lymph Node Detection Method

Yoshihiko Nakamura[a], Yukitaka Nimura[a], Takayuki Kitasaka[b], Shinji Mizuno[b], Kazuhiro Furukawa[c], Hidemi Goto[c], Michitaka Fujiwara[c], Kazunari Misawa[d], Masaaki Ito[e], Shigeru Nawano[f], Kensaku Mori[a,g]

[a]Information & Communications Headquarters, Nagoya University, Furo-cho, Chikusa-ku, Nagoya, 464-8603, Japan;
[b]School of Information Science, Aichi Institute of Technology, 1247 Yachigusa, Yakusa Cho, Toyota City, Aichi, 470-0392, Japan;
[c]Graduate School of Medicine, Nagoya University, 65, Tsurumai-cho, Syowa-ku, Nagoya, Aichi, 466-8550, Japan;
[d]Aichi Cancer Center Hospital, 1-1 Kanokoden, Chikusa-ku, Nagoya, Aichi, 464-8681, Japan;
[e]National Cancer Center Hospital East, Kashiwanoha, 6-5-1, Kashiwa, Chiba, 277-8577, Japan;
[f] International University of Health and Welfare Mita Hospital, 1-4-3 Mita, Minato-ku, Tokyo, 108-8329, Japan;
[g]Graduate School of Information Science, Nagoya University, Furo-cho, Chikusa-ku, Nagoya, 464-8603, Japan;

ABSTRACT

This paper presents an investigation of optimal feature value set in false positive reduction process for the automated method of enlarged abdominal lymph node detection. We have developed the automated abdominal lymph node detection method to aid for surgical planning. Because it is important to understand the location and the structure of an enlarged lymph node in order to make a suitable surgical plan. However, our previous method was not able to obtain the suitable feature value set. This method was able to detect 71.6% of the lymph nodes with 12.5 FPs per case. In this paper, we investigate the optimal feature value set in the false positive reduction process to improve the method for automated abdominal lymph node detection. By applying our improved method by using the optimal feature value set to 28 cases of abdominal 3D CT images, we detected about 74.7% of the abdominal lymph nodes with 11.8 FPs/case.

Keywords: computer aided surgery, lymph node detection, local intensity structure analysis, support vector machine

1. INTRODUCTION

Detection of abdominal lymph nodes from pre-operative CT volumes is important process for the pre-operative diagnosis of cancer-related surgery. In the abdominal cancer surgery, surgeons must resect not only tumors and metastases but also lymph nodes that have the possibility of metastasis. This procedure is called as lymphadenectomy or lymph node dissection. Insufficient lymphadenectomy has high risk for recurrence. However, excessive resection decreases patient's post-operative quality of life. Therefore, it is important to understand the

Further author information: (Send correspondence to Y. Nakamura)
Y. Nakamura: E-mail: ynakamura@mori.m.is.nagoya-u.ac.jp, Phone number: +81 (0)52 789 5688
K. Mori: E-mail: kensaku@is.nagoya-u.ac.jp, Phone number: +81 (0)52 789 5689

location and the structure of a lymph node in order to make a suitable surgical plan. An automated detection method for enlarged lymph nodes is very helpful for the preoperative diagnosis to decide the resection area.

Automated lymph node detection methods are proposed by several research groups.[1–4] The mediastinal lymph nodes detection methods are proposed by Feulner et al.[2] and Feuerstein et al.[3] Feulner et al.[2] proposed a method based on a spacial prior probability to detect mediastinal lymph nodes. Feuerstein et al.[3] proposed a method based on the probabilistic atlas showing the existences of mediastinal lymph nodes. These methods utilize the location information of mediastinal lymph nodes. However, in abdominal regions, the organs, blood vessels, and lymph nodes move easily according to a patient's posture. Therefore, the location information of lymph nodes is inefficient for detecting abdominal lymph nodes. Axillary and abdominal lymph nodes detection methos are proposed by Barbu et al.[1] which is based on the appearance of lymph nodes. This method can detect lymph nodes at high accuracy by using 3-D Haar-like features and gradient information. Also mediastinal and abdominal lymph node detction method was proposed by Roth et al.[4] based on convolutional neural network, by Seff et al.[?] using 2D images of lymph nodes. However, these methods target abdominal lymph nodes whose diameters are over 10 mm.

In contrast to these methods, we detect abdominal lymph nodes over 5 mm in diameter by a detection method based on the estimation and the classification of local intensity structures. Abdominal lymph nodes over 5 mm in diameter are more effective to diagnose abdominal lymph nodes metastasis. However, the detection results include many false positives (FPs) in the intestines and the veins.[5] This is because FP reduction based on lymph node size becomes much was critical. Moreover, we have tried to improve this detection method with an additional FP reduction process based on feature analysis.[6] However, this method was not able to obtain the suitable feature value set. This method was able to detect 71.6% of the lymph nodes with 12.5 FPs per case. And the number of features which is selected or deselected by the selection method is 20 from 87 features. In this paper, we investigate the optimal feature value set by using feature selection methods.

In Section 2, we describe our lymph node detection method and the detail of the feature selection method to investigate the optimal feature value set. The experimental results and discussion are described in Section 3 and 4, respectively.

2. METHOD

2.1 Overview

Our lymph node detection method consists of two processes: candidate lymph node detection and false positive reduction.[5] In the candidate lymph node detection, the blob-like structure enhancement (BSE) filter based on local intensity structure analysis detects the candidates of enlarged lymph nodes. In false positive reduction, the candidate regions are classified into lymph nodes and FPs based on the feature analysis. In this process, the classifier is constructed using the set of the feature values. In this paper, we optimize the set of feature values by investigating each feature value using the sequential feature selection method. The sequential feature selection method is the standard method. We utilize these selection methods to obtain the effectiveness of each feature.

2.2 Candidate lymph node detection and FP reduction

In order to enhance lymph nodes, a BSE filter based on Hessian analysis is applied to the abdominal CT image. The filter calculates the blob-like value of each voxel by using the combination of magnitudes of the eigenvalues of Hessian matrix. The candidate lymph node which is extracted by the thresholding process for the enhanced image by the BSE filter. However, the candidate region is not whole lymph node region. In order to extract whole lymph node region, the region growing technique are utilized.

FP reduction process utilizes a classifier based on SVM, which is implemented by Chang et al.[7] Table 1 shows the part of the typical feature value which is utilized in the classifier. They consist of two types of measurements: the texture and shape information. The texture information is calculated by the intensity value of the candidate regions. The lymph nodes are often surrounded by low-intensity structures. On the other hand, the FP such as the part of the intestines or veins connects the similar intensity region. Therefore, we utilize the texture information of the expanding candidate region and the surrounding region of the candidate region by subtracting the regions of the expanding candidate region. The shape information is calculated by the volume

and the surface of each candidate region. The enlarged lymph nodes are spherical or ellipsoidal. Therefore, if the sphericity of the candidate region is high, the candidate region has a high probability to be a lymph node. We investigate the optimal the set of feature values by the feature selection method in shown below.

2.3 Feature Selection method

The feature selection process can be expressed as

$$J(W) = \max_{Z \subseteq Y, \|Z\|=d} J(Z), \tag{1}$$

where W is the set of optimal feature values, Y is the set of all feature values, Z is a set of feature values, d is the number of feature value of Z, and J is the evaluation function. In this paper, we utilize the specificity of the discrimination results in the FP reduction process as the evaluation function.

There are many feature selection methods to optimize the set of feature value. In this paper, we use two simple sequential selection methods which are sequential forward selection (SFS) method and sequential backward selection (SBS). Because, our purpose of this work includes not only the improvement of the detection accuracy but also the development of new feature value at the future.

The SFS select the set of feature values by increase one by one which feature value can increase the evaluation function.

Input: $\mathrm{Z}_0 = \{\ \emptyset\ \}$
Output: subset Z_k
1 $k \leftarrow 1$
2 **repeat**
3 $x^+ = \arg\max_{x \notin Z_k} J(Z_k + x)$
4 $Z_{k+1} = Z_k + x^+$
5 $k \leftarrow k + 1$
6 **until** $J(Z_k)$ satisfies evaluation value

Algorithm 1. Sequential forward selection method

Where + shows the feature x is added to the set Z_k. The feature value x which maximizes the evaluation function $J(Z_k + x)$ adds to the set of the feature value Z. So, x can be assumed that the efficient feature value to improve detection accuracy.

The SBS selects the set of feature values by decrease one by one which feature value can increase the evaluation function.

Input: $\mathrm{Z}_0 = \mathrm{Y}$
Output: subset Z_k
1 $k \leftarrow D$
2 **repeat**
3 $x^- = \arg\max_{x \in Z_k} J(Z_k - x)$
4 $Z_{k-1} = Z_k - x^-$
5 $k \leftarrow k - 1$
6 **until** $J(Z_k)$ satisfies evaluation value

Algorithm 2. Sequential backward selection method

Where − shows the feature x is subtracted from the set Z_k and D is the number of feature value of Y. The feature value x which maximizes the evaluation function $J(Z_k - x)$ subtracts from the set of the feature value Z.

Table 1 Typical feature values

Type of feature	Feature values
Shape related feature value	Ratio of volume and surface area, Ratio of major axis and miner axis, Sphericity, Inscribed sphericity, Circumscribed sphericity, Cross-section area of bounding box
Texture related feature value*	Average, Variance, Maximum value, Minimum value, Median value, First quartile, Third quartile, Degree of kurtosis and degree of skewness

* Texture related feature values are calculated by candidate region and/or its surrounding region.

3. EXPERIMENTS

We investigate the optimal feature value set by using feature selection methods. We evaluated each feature value set by using of 28 cases of 3-D abdominal CT images, including five colorectal cancer and 23 stomach cancer cases, by leave-one-patient-out cross validation. We performed the leave-one-patient-out cross validation in each step of the feature selection methods. CT images were taken by multi-detector row CT scanners(512 $\times$ 512 pixels, 238-521 slices, 0.586-0.782 mm pixel spacing, 0.5-1.0 mm reconstruction pitch). The ground truth of the 26 cases was created by medical doctors, and that of the other two cases was created by two engineers who are experts in lymph node detection. The number of target lymph nodes is 95. The parameter of the detection method is described in the previous method.[5] The maximum number of selected and deselected feature values are 60. SFS utilize 1 to 60 feature values. SBS utilize 86 to 25 feature values.

Experimental results showed that the TP fraction was 74.7% (71/95) and the number of FPs per case was 11.8 using 27 feature values selected by SFS. Figure 1 shows the precision rate that are results utilized selected and deselected feature values by SFS and SBS method respectively. Figure 2 shows an example of TP case and Figure 3 shows an example of FP case when utilize optimal feature value set. The green region shows TP and the yellow region shows FP.

4. DISCUSSION

As shown in Fig.1, the feature values that is efficient to increase the detection accuracy can be selected by SFS. The efficiency of the selected feature values and the combination of the selected feature values by SFS will cause such results. The best result is indicated by yellow arrow when the number of feature values is 27. Although the number of the shape-related feature values prepared in this paper is 12, 9 shape-related feature values are selected from 12 prepared feature values. An one third of the optimal feature value set is the shape-related feature value. This indicates that shape-related feature values are efficient in the classification process. On the other hand, the number of the shape-related feature values that is deselected as the inefficient feature by SBS is three out of 50. These experimental results indicate that the shape-related feature value is important and effective to improve FP reduction process.

The selected texture-related feature values in the optimal feature value set consists of four values calculated from candidate region and 14 values calculated from the surrounding region. Furthermore, texture-related feature values of surrounding regions contributed in the improvement of the precession rate (Feature values 18, 21, 22, 23). These experimental results indicate the surrounding regions of the candidate region is also effective.

Additionally, the SFS and the SBS method can fall into a local minimum. In Fig.1, the precision rate is different between SFS and SBS when the same number of features are in feature set. This indicates that SFS and/or SBS method may fall in a local solution. We plan to avoid these problems by utilizing sequential floating selection methods or similar.

Figure 2 shows that the proposed method was able to detect abdominal lymph nodes of various sizes. Figure 3 shows that the shape and the texture of abdominal lymph nodes are very similar to the remained FP's one. Therefore, we have to develop new features to distinguish such FPs.

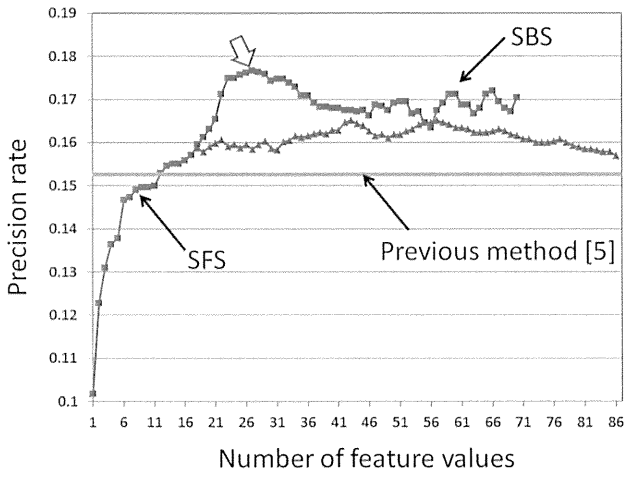

Figure 1 Precision rate that are results utilized selected and deselected feature values. Blue line shows results of SFS. Red line shows results of SBS. Green line shows precision rate when utilize whole feature values. Yellow arrow indicates best accuracy.

5. CONCLUSIONS

This paper presents the investigation of the optimal feature value set in FP reduction process for automated abdominal lymph node detection. We were able to improve the TP rate from 71.6% to 74.7% and reduce the FPs from 12.5 per case to 11.8 per case by using the optimal feature value set. Future work includes improvement of the feature selection method using another selection method and development of new feature value from the features which are contribute to the detection accuracy.

ACKNOWLEDGMENTS

The authors thank our colleagues for suggestions and advices. Parts of this research were supported by the Grant-In-Aid for Scientific Research from the Ministry of Education (MEXT), Japan Society for the Promotion of Science (JSPS) KAKENHI Grant Number 21103006, 25242047, 26560255, 26108006, the Health Labour Sciences Research Grant, and the Kayamori Foundation of Informational Science Advancement.

REFERENCES

[1] Barbu, A., Suehling, M., Xu, X., Liu, D., Zhou, S., and Comaniciu, D., "Automatic detection and segmentation of lymph nodes from ct data," *IEEE Trans Med Imaging* **31**, 240–250 (2012).

[2] Feulner, J., Zhou, S. K., Hammon, M., Hornegger, J., and Comaniciu, D., "Lymph node detection and segmentation in chest ct data using discriminative learning and a spatial prior," *Medical Image Analysis* **17**, 254–270 (2012).

[3] Feuerstein, M., Glocker, B., Kitasaka, T., Nakamura, Y., Iwano, S., and Mori, K., "Mediastinal atlas creation from 3-d chest computed tomography images: application to automated detection and station mapping of lymph nodes," *Medical Image Analysis* **16**, 63–74 (2012).

[4] Roth, H., Lu, L., Seff, A., Cherry, K., Hoffman, J., Wang, S., Liu, J., Turkbey, E., and Summers, R., "A new 2.5d representation for lymph node detection using random sets of deep convolutional neural network observations," *Lecture Notes in Computer Science* **8673**, 520–527 (2014).

[5] Seff, A., Lu, L., Cherry, K., Roth, H., Liu, J., Wang, S., Hoffman, J., Turkbey, E., and Summers, R., "2d view aggregation for lymph node detection using a shallow hierarchy of linear classifiers," **8673**, 544–552 (2014).

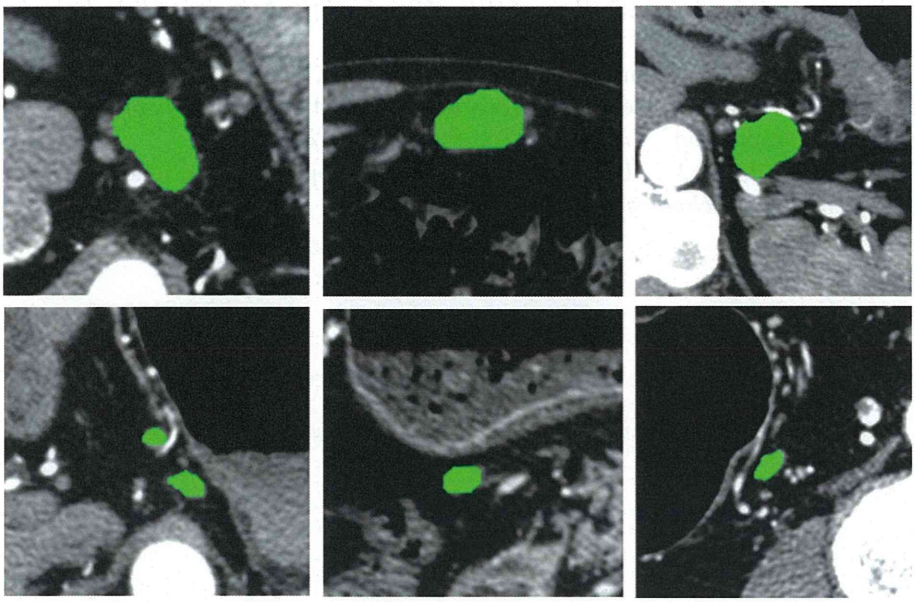

Figure 2 Examples of TP (Upper row: large TP, Lower row: small TP).

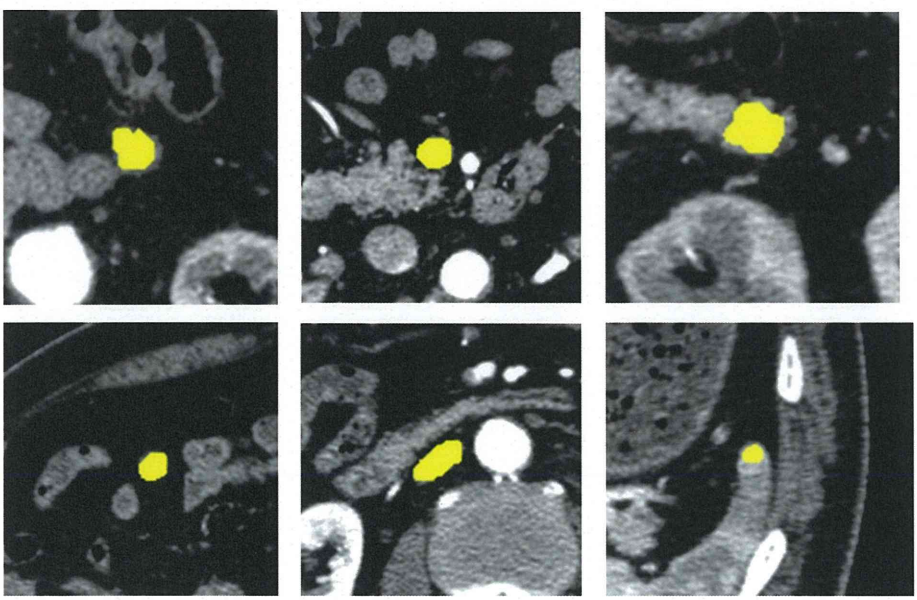

Figure 3 Examples of FP (left column: part of intestine, middle column: part of vein, right column: part of abdominal organ).

[6] Nakamura, Y., Kitasaka, T., Mizuno, S., Furukawa, K., Goto, H., Fujiwara, M., Misawa, K., Ito, M., Nawano, S., and Mori, K., "Automatic abdominal lymph node detection method based on local intensity structure analysis from 3-d x-ray ct images," *Proc. SPIE 8670, Medical Imaging 2013: Computer-Aided Diagnosis* , 86701K (2013).

[7] Nakamura, Y., Kitasaka, T., Mizuno, S., Furukawa, K., Goto, H., Fujiwara, M., Misawa, K., Ito, M., Nawano, S., and Mori, K., "A study on feature analysis in false positive reduction process of automated abdominal lymph node detection method," *Int J CARS* **9**, S225–S227 (2014).

[8] Chang, C. C. and Lin, C. J., "Libsvm: a library for support vector machines," *ACM Transactions on Intelligent Systems and Technology* **2**, 27:1–27:27 (2011).

Automated branching pattern report generation for laparoscopic surgery assistance

Masahiro ODA[a], Tetsuro MATSUZAKI[a], Yuichiro HAYASHI[b], Takayuki KITASAKA[c], Kazunari MISAWA[d], and Kensaku MORI[b,a]

[a]Graduate School of Information Science, Nagoya University, Furo-cho, Chikusa-ku, Nagoya, Aichi, 464-8603, Japan;
[b]Information and Communications, Nagoya University,
[c]Faculty of Information Science, Aichi Institute of Technology,
[d]Aichi Cancer Center Hospital

ABSTRACT

This paper presents a method for generating branching pattern reports of abdominal blood vessels for laparoscopic gastrectomy. In gastrectomy, it is very important to understand branching structure of abdominal arteries and veins, which feed and drain specific abdominal organs including the stomach, the liver and the pancreas. In the real clinical stage, a surgeon creates a diagnostic report of the patient anatomy. This report summarizes the branching patterns of the blood vessels related to the stomach. The surgeon decides actual operative procedure. This paper shows an automated method to generate a branching pattern report for abdominal blood vessels based on automated anatomical labeling. The report contains 3D rendering showing important blood vessels and descriptions of branching patterns of each vessel. We have applied this method for fifty cases of 3D abdominal CT scans and confirmed the proposed method can automatically generate branching pattern reports of abdominal arteries.

Keywords: Anatomical labeling, laparoscopic surgery, blood vessels, gastric cancer, diagnostic report

1. INTRODUCTION

Understanding of blood vessel structure for each patient is a crucial task in pre-operative diagnosis. Gastrointestinal cancer is common disease especially in Asian countries. Gastrointestinal cancers of early stages are nowadays are resected by laparoscopic surgery. In gastrectomy using a laparoscope, it is very important to understand branching structure of the abdominal arteries and veins, which feed and drain specific abdominal organs including the stomach, the liver and the pancreas.[1] Since there are many variations in branching patterns in the abdominal blood vessels, a surgeon needs to understand the branching patterns of the abdominal blood vessels of a patient to be treated at the preoperative diagnostic stage. For example, in the real clinical field, a surgeon creates a diagnostic report of the patient anatomy as shown in Fig. 1. This report summarizes the branching patterns of the blood vessels which feed and drain the stomach. It depicts a key frame of 3D rendering of the abdominal blood vessels and shows short description of branching structure of key blood vessels. Based on such reports, the surgeon decides actual operative procedure like blood vessel clipping in gastrectomy.

Many blood vessel extraction methods from medical images have been proposed.[2–5] By using blood vessel regions extracted by the extraction methods, anatomical labeling can be performed. There are several reports on automated anatomical labeling of the abdominal blood vessels. Hoang et al. presented automated method for anatomical labeling of the abdominal arteries, which is based on the machine learning technique.[6] This method is able to assign anatomical names of each branch of the abdominal arteries by constructing the classifier that outputs anatomical names based on features computed for each branch. Matsuzaki et al. presented a method

Further author information: (Send correspondence to M. Oda)
M. Oda: E-mail: moda@mori.m.is.nagoya-u.ac.jp, Telephone: +81 (0)52 789 5688
T. Kitasaka: E-mail: kitasaka@aitech.ac.jp, Telephone: +81 (0)565 48 8121
K.Mori: E-mail: kensaku@is.nagoya-u.ac.jp, Telephone: +81 (0)52 789 5689

Figure 1. Sample of diagnostic report about branching pattern of blood vessels created by surgeon.

for anatomical labeling of the abdominal veins.[7] This method is also utilizing a machine learning technique and is extensible for the abdominal veins. Suzuki et al. tried automated anatomical labeling by considering organs connecting to the blood vessels.[8] It would be very helpful for laparoscopic surgery if we could generate diagnostic report of branching patterns of the blood vessels based on automated anatomical labeling. However there is no report on automated generation of diagnostic report of the abdominal blood vessels.

This paper tries to automatically generate diagnostic reports of blood vessel branching patterns of a patient who will have gastrectomy surgery. Blood vessel regions and anatomical labels of them are obtained from a CT volume. A key frame of blood vessels and a branching pattern summary are automatically generated from the blood vessel regions and the anatomical labels. The key frame and the branching pattern summary are included in an automatically generated diagnostic report.

2. METHOD

2.1 Overview

Blood vessels considered in generating a diagnostic report are listed in Tables 1 and 2. Here, we describe the set of anatomical names shown in the tables as N.

The proposed method consists of the following four steps: (a) preprocessing, (b) automated anatomical labeling, (c) key frame rendering, (d) branching pattern summary generation, (e) diagnostic report output about blood vessels. In this paper, a tree structure of the abdominal blood vessels is express by the graph representation. Each edge of the graph represents each branch of the blood vessels. Anatomical names are assigned to each edge of the graph.

To determine necessary information in the diagnostic report, we checked diagnostic reports that are manually made by a surgeon and discussed about necessary information. Based on our discussions, the following information are selected: (a) 3D key frame, (b) information about each branch and (c) positional relationship between CHA and LGV. We generated the following information for each branch: anatomical name, anatomical name of the parent branch and the position of the branching point. Since the positional relationship of CHA and LGV topologically differs among patients and these blood vessels are important in gastrectomy (CHA runs anterior side than LGV or opposite positional relation), we generate a special report for these blood vessels.

Table 1. Abdominal arteries described in a diagnostic report.

Abdominal artery name	Short name
abdominal aorta	Ao
celiac artery	CA
common hepatic artery	CHA
proper hepatic artery	PHA
left hepatic artery	LHA
right hepatic artery	RHA
gastroduodenal artery	GDA
left gastric artery	LGA
right gastric artery	RGA
left gastro-epiploic artery	LGEA
right gastro-epiploic artery	RGEA
splenic artery	SA
superior mesenteric artery	SMA
inferior mesenteric artery	IMA
left renal artery	LRA
right renal artery	RRA
left common iliac artery	LCIA
right common iliac artery	RCIA
left external iliac artery	LEIA
right external iliac artery	REIA
left internal iliac artery	LIIA
right internal iliac artery	RIIA

Table 2. Hepatic portal veins described in a diagnostic report.

Hepatic portal vein name	Short name
portal vein	PV
superior mesenteric vein	SMV
inferior mesenteric vein	IMV
splenic vein	SV
left gastric vein	LGV
gastro-colic trunk	GCT
left gastro-epiploic vein	LGEV
right gastro-epiploic vein	RGEV

2.2 Branching pattern report generation

2.2.1 Preprocessing

We extract blood vessel regions from the CT volume. The upper abdominal arteries and portal vein systems are targets of the proposed method. Region-growing based method followed by manual correction is utilized here to extract blood vessel regions. These blood vessel regions are thinned[10] to obtain the medial lines. The graph structure G is constructed from the thinned results and is expressed as $G = (\mathbf{V}, \mathbf{B})$. Here, $\mathbf{V}$ shows a set of ends or branching nodes of the graph and $\mathbf{B}$ represents a set of paths of branches. The path is represented by a set of voxels forming a branch.

2.2.2 Anatomical labeling

Anatomical labeling is performed by the method based on the optimum branching pattern selection.[7] Although this method basically performs anatomical labeling based on the machine learning approach, we determine anatomical labels for each branch on the graph showing possible branching pattern variations. After this step, each branch (edge) of the tree structure has its anatomical name shown in Tables 1 and 2.

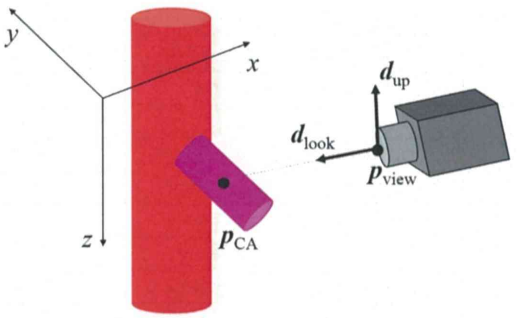

Figure 2. Viewpoint and view direction set up. Virtual camera is oriented so that it looks at CA.

2.2.3 Key frame rendering

Diagnostic report includes one or more pictures that enable a surgeon to understand branching patterns and running direction of blood vessels. Since it is hard to understand them from 2D slices, it is needed to generate 3D rendering of blood vessel regions extracted in the prepossessing step. The important point to render such images is determination of the viewpoint and the view direction. Once the viewpoint and the view direction are determined, 3D key frame is rendered by the volume rendering technique.[9]

Since the proposed method mainly focuses on diagnostic report generation for assisting gastrectomy, it is required to show important blood vessels in gastrectomy including the gastric artery, the hepatic artery and the gastric vein. We need to automatically compute the viewpoint and the view direction of the virtual camera of the volume rendering for enabling us to see such blood vessels on a 3D rendered image.

Most of the gastric and the hepatic arteries are children or grandchildren branches of the CA. The gastric vein runs parallel to the gastric artery. Hence, we set CA as the point of interest and the viewpoint is located at the upper-left side of the CA. The viewpoint $\mathbf{p}_{\text{view}}$, the view direction $\mathbf{d}_{\text{look}}$, and the up direction $\mathbf{d}_{\text{up}}$ is determined by the following way. These positional relationship is shown in Fig. 2.

First, we look for a branch b whose anatomical name is CA. Then the middle point of b is considered as the point of interest $\mathbf{p}_{\text{CA}}$. The viewpoint $\mathbf{p}_{\text{view}}$ is located at the upper-left side of CA and is calculated as

$$\mathbf{p}_{\text{view}} = \mathbf{p}_{CA} + (a_1 w, b_1 h, c_1 d)^T, \tag{1}$$

where w, h and d mean the length along the right to the left direction, the anterior to the posterior direction and head-to-foot direction. a_1, b_1 and c_1 are constants adjusting the camera location. The view direction $\mathbf{d}_{\text{look}}$ of the camera can be easily computed by the relationship between the camera position $\mathbf{p}_{\text{view}}$ and the point of interest $\mathbf{p}_{\text{CA}}$. $\mathbf{d}_{\text{look}}$ is calculated as

$$\mathbf{d}_{\text{look}} = \frac{1}{|\mathbf{p}_{\text{CA}} - \mathbf{p}_{\text{view}}|} |\mathbf{p}_{\text{CA}} - \mathbf{p}_{\text{view}}| \,. \tag{2}$$

The up direction of the virtual camera is set so that it heads to the head direction. It is computed by

$$\mathbf{d}_{\text{up}} = R\left(\mathbf{d}_{\text{view}}, \mathbf{d}_{\text{view}} \times \mathbf{d}_{\text{head}}, \frac{\pi}{2}\right), \tag{3}$$

where $R(\mathbf{a}, \mathbf{b}, \theta)$ means the rotation of the vector $\mathbf{a}$ around the axis $\mathbf{b}$ in the degree of θ. $\mathbf{d}_{\text{head}}$ shows the foot-to-head direction and defined as $\mathbf{d}_{\text{head}} = (0, 0, -1)^T$.

If we cannot find the CA in anatomical labeling results, we calculate the viewpoint and the view direction as

$$\mathbf{p}_{\text{view}} = \mathbf{p}_{CA} + (a_2 w, b_2 h, c_2 d)^T, \tag{4}$$
$$\mathbf{d}_{\text{look}} = (0, 1, 0)^T, \tag{5}$$
$$\mathbf{d}_{\text{head}} = (0, 0, -1)^T. \tag{6}$$
$$\tag{7}$$

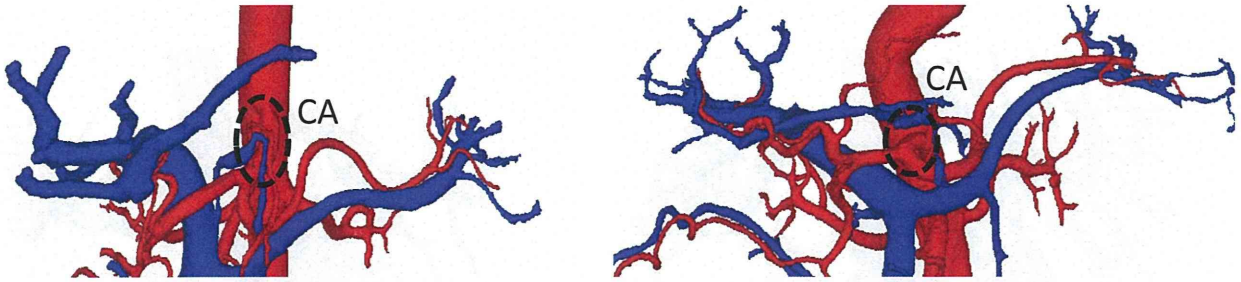

Figure 3. Examples of automatically generated 3D key frame images. Positions of the CAs are indicated in these figures.

Then we generate a key frame image by the volume rendering using the viewpoint and the view direction parameters calculated above. Figure 3 shows examples of key frame images.

2.2.4 Branching pattern summary generation

It is important to understand the base branch (parent or grandparent branch) of each blood vessel, distances from the base branch to a target branch and branching positions in pre-operative diagnosis. The proposed method generates such report as textual information. Branching position shows the branching location of the target branch such as branching on the way of the base branch or branching at the end point of the base branch.

Branching information For each anatomical name $v \in N$, we find the actual branch $b \in \mathbf{B}$ having the anatomical name v. Then the base branch $\hat{b}$ of b is found from the tree structure of the blood vessel region of the input volume. We output the anatomical name of v and the anatomical name of the base branch $\hat{b}$ on the report. If we cannot find anatomical name v in the anatomical labeling results, the report shows v *does not exist.*

We also output the branching point information on the report. If the starting point $\mathbf{s}_b$ of the branch b having anatomical name v coincides with the end point $\mathbf{e}_{\hat{b}}$ of the origin branch $\hat{b}$ having the anatomical name $\hat{v}$, the report for the branch v shows *bifurcate from the end of* $\hat{v}$. If not, we compute the distance l from the start point $\mathbf{s}_{\hat{b}}$ of the base branch $\hat{b}$ having the anatomical name $\hat{v}$ to the starting point $\mathbf{s}_b$ of the branch b having anatomical name v along the medial line of the blood vessel regions. In this case, the report shows *bifurcate at* l *mm point from the base point of* $\hat{v}$.

Topological information The proposed method also outputs topological relationship of the CHA and LGV. Let P_{CHA} and P_{LGV} be a set of voxels forming the path of the branch having the name CHA and a set of voxels forming the path of the branch having the name LGV, respectively. We compute two points $\mathbf{p}^*$ and $\mathbf{q}^*$ by

$$(\mathbf{p}^*, \mathbf{q}^*) = \mathrm{argmin}_{\mathbf{p}\in P_{\mathrm{CHA}}, \mathbf{q}\in P_{\mathrm{LGV}}} \quad = \quad \sqrt{(p_x - q_x)^2 + (p_z - q_z)^2}, \tag{8}$$

where $\mathbf{p}, \mathbf{q}$ are $\mathbf{p} = (p_x, p_y, p_z)$ and $\mathbf{q} = (q_x, q_y, q_z)$. All points described here exist in the CT coordinate system. In the CT coordinate system, the x-axis direction is the left to the right direction, the y-axis direction is the posterior to the anterior direction and the z-axis direction is the head to the tail direction of the human body. $\mathbf{p}^*, \mathbf{q}^*$ means a pair of voxels whose distance becomes minimum on the x-z plane where all voxels are projected. The x-z plane is a coronal slice in the CT coordinate system. If the distance $\sqrt{(p_x^* - q_x^*)^2 + (p_z^* - q_z^*)^2}$ between two voxels $\mathbf{p}^*$ and $\mathbf{q}^*$ on the x-z plane becomes smaller than a given threshold value t_{cross}, we consider that the CHA and LGV are in the skew position. In this case, if $p_y^* < q_y^*$, we determine the CHA runs the posterior side and the LGA runs the anterior side. Also $p_y^* > q_y^*$, we determine the CHA runs the anterior side and the LGA runs the posterior side. This topological relation is also output on the report. If the distance is lower than t_{cross}, no information about the topological relationship of the CHA and LGA is output on the report.

2.2.5 Branching pattern report generation

Finally, we output all information generated in the previous sections as a report. The report contains a 3D rendering showing important blood vessels and description of branching patter of each vessel. The report file is coded by HTML file format and can be printed on a paper or can be displayed on computer display.

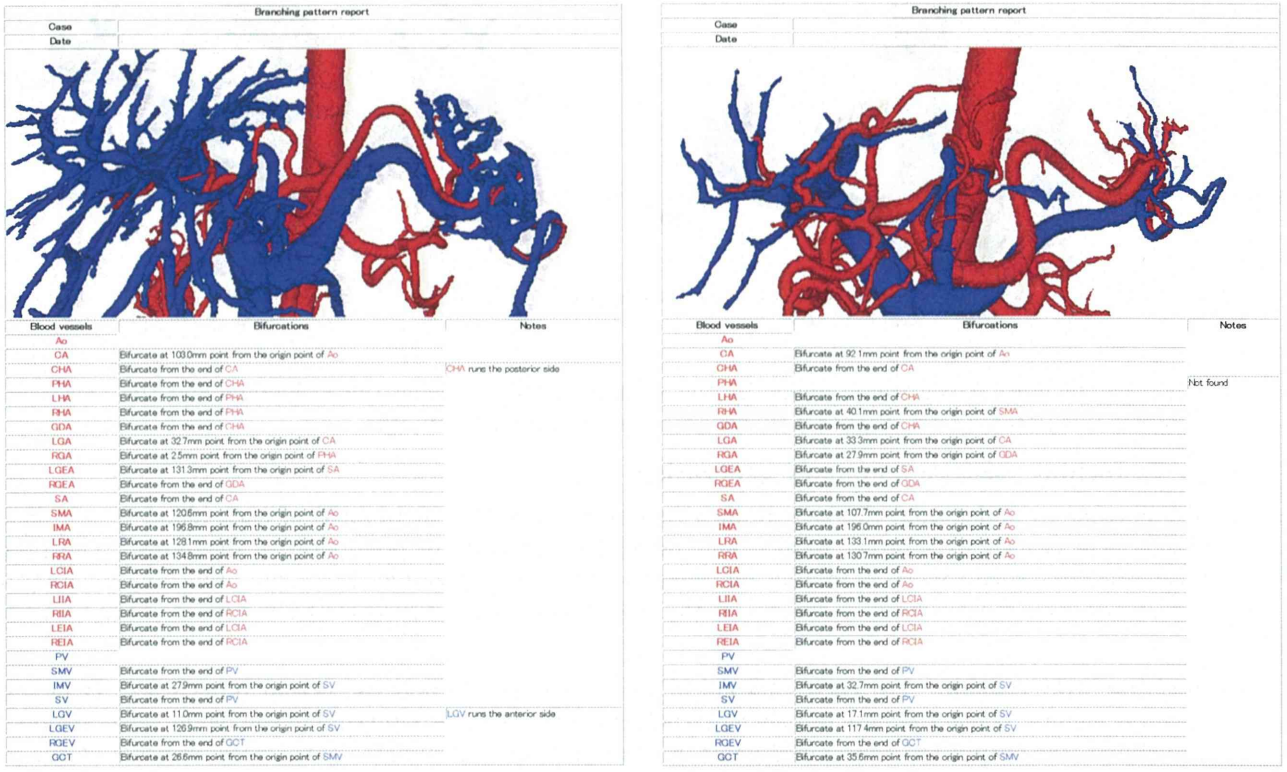

Branching pattern report

Case

Date

Blood vessels	Bifurcations	Notes
Ao		
CA	Bifurcate at 103.0mm point from the origin point of Ao	
CHA	Bifurcate from the end of CA	CHA runs the posterior side
PHA	Bifurcate from the end of CHA	
LHA	Bifurcate from the end of PHA	
RHA	Bifurcate from the end of PHA	
GDA	Bifurcate from the end of CHA	
LGA	Bifurcate at 32.7mm point from the origin point of CA	
RGA	Bifurcate at 2.5mm point from the origin point of PHA	
LGEA	Bifurcate at 131.3mm point from the origin point of SA	
RGEA	Bifurcate from the end of GDA	
SA	Bifurcate from the end of CA	
SMA	Bifurcate at 120.6mm point from the origin point of Ao	
IMA	Bifurcate at 196.8mm point from the origin point of Ao	
LRA	Bifurcate at 128.1mm point from the origin point of Ao	
RRA	Bifurcate at 134.8mm point from the origin point of Ao	
LCIA	Bifurcate from the end of Ao	
RCIA	Bifurcate from the end of Ao	
LIIA	Bifurcate from the end of LCIA	
RIIA	Bifurcate from the end of RCIA	
LEIA	Bifurcate from the end of LCIA	
REIA	Bifurcate from the end of RCIA	
PV		
SMV	Bifurcate from the end of PV	
IMV	Bifurcate at 27.9mm point from the origin point of SV	
SV	Bifurcate from the end of PV	
LGV	Bifurcate at 11.0mm point from the origin point of SV	LGV runs the anterior side
LGEV	Bifurcate at 126.9mm point from the origin point of SV	
RGEV	Bifurcate from the end of GCT	
GCT	Bifurcate at 26.6mm point from the origin point of SMV	

Branching pattern report

Case

Date

Blood vessels	Bifurcations	Notes
Ao		
CA	Bifurcate at 92.1mm point from the origin point of Ao	
CHA	Bifurcate from the end of CA	
PHA		Not found
LHA	Bifurcate from the end of CHA	
RHA	Bifurcate at 40.1mm point from the origin point of SMA	
GDA	Bifurcate from the end of CHA	
LGA	Bifurcate at 33.3mm point from the origin point of CA	
RGA	Bifurcate at 27.9mm point from the origin point of GDA	
LGEA	Bifurcate from the end of SA	
RGEA	Bifurcate from the end of GDA	
SA	Bifurcate from the end of CA	
SMA	Bifurcate at 107.7mm point from the origin point of Ao	
IMA	Bifurcate at 196.0mm point from the origin point of Ao	
LRA	Bifurcate at 133.1mm point from the origin point of Ao	
RRA	Bifurcate at 130.7mm point from the origin point of Ao	
LCIA	Bifurcate from the end of Ao	
RCIA	Bifurcate from the end of Ao	
LIIA	Bifurcate from the end of LCIA	
RIIA	Bifurcate from the end of RCIA	
LEIA	Bifurcate from the end of LCIA	
REIA	Bifurcate from the end of RCIA	
PV		
SMV	Bifurcate from the end of PV	
IMV	Bifurcate at 32.7mm point from the origin point of SV	
SV	Bifurcate from the end of PV	
LGV	Bifurcate at 17.1mm point from the origin point of SV	
LGEV	Bifurcate at 117.4mm point from the origin point of SV	
RGEV	Bifurcate from the end of GCT	
GCT	Bifurcate at 35.6mm point from the origin point of SMV	

(a) (b)

Figure 4. Examples of branching pattern reports generated by the proposed method.

3. EXPERIMENTS

We evaluated our proposed method using subjective evaluation by a skilled surgeon. In the experiment, we utilized 50 cases of vasculatures annotated by an automated anatomical labeling method of abdominal blood vessels. The parameters utilized in the experiment were $t_{\mathrm{cross}} = 2$ mm, $a_1 = 0.1$, $b_1 = -0.3$, $c_1 = -0.3$, $a_2 = 0.45$, $b_2 = -0.5$, $c_2 = 0.25$, respectively. These parameters are selected based on our experiments.

Figure 4 shows examples of branching pattern reports generated by the proposed method. Table 3 shows parts of the branching pattern summary of the case shown in Fig. 4 (a). The topological relationship of the CHA and LGA is described in the notes column of the CHA and LGV rows. These reports were evaluated by a surgeon and his comments were: (a) The branching pattern report generated by the proposed method is useful to create surgical plans. (b) The report of topological relationship of the CHA and LGV is quite useful. Because it is important to understand their topological relationship to perform laparoscopic gastrectomy. (c) In order to understand vasculature intuitively, it is necessary to revise the representation of the branching point of some blood vessels. (d) Several rendered images or videos are needed. (e) It would be nice if we can have an interactive report system which enables surgeons to freely adjust observation information.

We also evaluated the recognition result of topological relationship of the CHA and LGV by visual inspections. In a case of crossing CHA and LGV, the proposed method reports correct positional relationship of these blood vessels. In no-crossing cases, the record about the relationship of CHA and LGV must be omitted. The recognition rate of topological relationship of CHA and LGV was 88.0%.

4. DISCUSSION

The surgeon's comments revealed that the branching pattern report generated by our method is useful in the surgical planning. The reports summarized by the proposed method included not only the visualization of

Table 3. Parts of the branching pattern summary of the case shown in Fig. 4 (a).

Blood vessel	Bifurcations	Notes
Ao		
CA	Bifurcate at 103.0mm point from the origin point of Ao	
CHA	Bifurcate from the end of CA	CHA runs the posterior side
PHA	Bifurcate from the end of CHA	
LHA	Bifurcate from the end of PHA	
RHA	Bifurcate from the end of PHA	
GDA	Bifurcate from the end of CHA	
SV	Bifurcate from the end of PV	
LGV	Bifurcate at 11.0mm point from the origin point of SV	LGV runs the anterior side
LGEV	Bifurcate at 126.9mm point from the origin point of SV	

patient' individual abdominal blood vessels but also the recording of the analyzed vasculature. Especially, the topological relationship of the CHA and LGV is one of important functions. The experimental result shows that the proposed method can give surgeons correct information of the topological relationship, if anatomical labeling of blood vessels worked properly. Therefore, this function recognizing topological relationship of the CHA and LGV is practical in the clinical field. The recognition rate of topological relationship was 88.0%. The failure reports were mainly caused by miss-labeling in the anatomical labeling method. About five reports contained incorrect information about CHA and LGV relationship in failure reports. Correct reports were generated when the proposed method utilize correct labeling results. In another case, the correct report can be obtained by adjusting t_{cross}.

Although information of the branching point of a blood vessel is also important, it is necessary to improve the presentation method of the branching point. The optimum representations are blood vessel specific. Therefore, we need to consider that the development of blood vessel specific representation.

In this paper, the proposed method visualized only one image to generate a branching pattern report. However, this approach creates a problem such as an occlusion of the blood vessels. For example, parts of CA are occluded by other blood vessels in Fig. 4 (b). In order to solve this problem, we need to create several visualized image or videos. An interactive report system which enables surgeons to freely adjust a viewpoint and observation information is other way to solve the problem.

5. CONCLUSIONS

This paper shows an automated method to generate a branching pattern report for the abdominal blood vessels based on automated anatomical labeling. The report contains 3D rendering showing important blood vessels and descriptions of branching patterns of each vessel. We have applied this method for fifty cases of 3D abdominal CT scans and confirmed the proposed method can automatically generate branching pattern reports of the abdominal blood vessels. Future work includes introduction of an expression that is intuitive to surgeons, adjustment to the viewpoint that is easy to understand vasculature in the visualization, application to a lot of cases, and improvement of the accuracy of analyzing branching pattern of the abdominal blood vessels.

ACKNOWLEDGMENTS

Parts of this research were supported by the MEXT, the JSPS KAKENHI Grant Numbers 21103006, 25242047, 26108006, 26560255, and the Kayamori Foundation of Informational Science Advancement.

REFERENCES

[1] Maruyama, K., Okabayashi, K., Kinoshita, T., "Progress in gastric cancer surgery in Japan and its limits of radicality," World Journal of Surgery 11, 419–425 (1987)

[2] Schmitt, H., Grass, M., Rasche, V., Schramm, O., Haehnel, S., Sartor, K., "An X-Ray-Based Method for the Determination of the Contrast Agent Propagation in 3-D Vessel Structures," IEEE Transactions on Medical Imaging, 21(3), 251–262 (2002)

[3] Xiao, C., Staring, M., Wang, Y., Shamonin, D. P., Stoel, B. C., "Multiscale Bi-Gaussian Filter for Adjacent Curvilinear Structures Detection With Application to Vasculature Images," IEEE Transactions on Image Processing, 22(1), 174–188 (2013)

[4] Schneider, M., Hirsch, S., Weber, B., Szekely, G., Menze, B. H., "Joint 3-D vessel segmentation and centerline extraction using oblique Hough forests with steerable filters," Medical Image Analysis, 19(1), 220–249 (2014)

[5] Cherry, K. M., Peplinski, B., Kim, L., Wang, S., Lu, L., Zhang, W., Liu, J., Wei, Z., Summers, R. M., "Sequential Monte Carlo tracking of the marginal artery by multiple cue fusion and random forest regression," Medical Image Analysis, 19(1), 164–175 (2014)

[6] Hoang, B. H., Oda, M., Jiang, Z., Kitasaka, T., Misawa, K., Fujiwara, M., Mori, K., "A study on automated anatomical labeling to arteries concerning with colon from 3D abdominal CT images," Proceedings of SPIE 7962, 79623R–79623R-9 (2011)

[7] Matsuzaki, T., Oda, M., Kitasaka, T., Hayashi, Y., Misawa, K., Mori, K., "Automated anatomical labeling of abdominal arteries and hepatic portal system extracted from abdominal CT volumes," Medical Image Analysis, 20(1), 152–161 (2015)

[8] Suzuki, Y., Okada, T., Hori, M., Yokota, F., Linguraru, M., Tomiyama, N., Sato, Y., "Automated anatomical labeling of abdominal arteries from CT data based on optimal path finding between segmented organ and aorta regions: A robust method against topological variability," Intetnational Journal of CARS 7, S47–S48 (2012)

[9] Levoy, L., "Display of surfaces from volume data," IEEE Transactions on Compututer Graphphcs and Applications 8(3), 29–37 (1988)

[10] Saito, T., Toriwaki, J., "New algorithms for n-dimensional Euclidean distance transformation," Pattern Recognition, 27(11), 1551–1565 (1994)